SAND2011-4913C

PIC SIMULATIONS OF POWER FLOW IN A LINEAR TRANSFORMER DRIVER FOR RADIOGRAPHIC APPLICATIONS *

T. D. Pointon[ξ], D. B. Seidel, J. J. Leckbee and B. V. Oliver
Sandia National Laboratories, PO Box 5800, Mail Stop 1152
Albuquerque, NM 87185 USA

Abstract

The 7 cavity, 1 MV linear transformer driver for radiography at Sandia National Laboratories has recently been upgraded to 21 cavities with an output voltage of 2.5 MV. In this paper, results from 2-D, r-z particle-in-cell simulations of the full 21 cavity system are presented. Each cavity feed is driven with its own external RLC circuit that is independently triggered, and has a realistic 45° slanted vacuum/insulator. Electrons are emitted from the central cathode with a conventional space-charge-limited emission model. Detailed diagnostics monitor electron loss to the anode, cavity conductors, and the insulators. The most significant and encouraging result is that the simulations have absolutely no electron loss to the insulators, even with large random variations in the trigger timing.

I. INTRODUCTION

The linear transformer driver (LTD) is a promising technology for building a compact, high-voltage driver for radiographic applications. Prototype 1 MV LTDs have been built at several sites for proof-of-principle experiments [1,2], but radiographic applications require higher voltage, V > 2 MV, and ideally much higher, 7 – 8 MV. A cause for concern is that at the higher voltage, there will be substantially greater electron flow current in the central magnetically insulated transmission line (MITL). The existing 1 MV LTD at Sandia National Laboratories has recently been upgraded to 21 series cavities with an output voltage of 2.5 MV [3]. This system is shown in Fig. 1. It consists of three groups of seven cavities. The inner surfaces of the cavities form the MITL anode at a radius of r_a = 14.5 cm. The cathode stalk inside the cavities consists of three uniform impedance sections with parameters shown in Table 1. There are relatively abrupt conical transitions between the sections; the first between cavities 6 and 7, and the second between cavities 13 and 14. This system provides the first opportunity to evaluate the effects of substantial electron flow in a multi-cavity driver at the low end of the voltage needed for radiography.

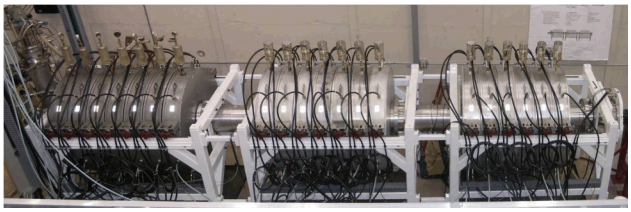

Figure 1. The 21 cavity LTD for radiography at Sandia. This system is approximately 7.5 m long and 1.5 m wide.

Table 1. Parameters of the three MITL sections.

Section	r_c(m)	Z_{vac}(Ω)	z-range (m)
1	0.1105	16.3	0 – 1.23
2	0.0826	33.7	1.44 – 3.53
3	0.0635	49.5	3.75 – 6.80

In this paper, we describe 2-D, azimuthally symmetric r-z PIC simulations of this system using the QUICKSILVER code [4].

II. SIMULATION SETUP

The simulation r-z geometry is shown in Fig. 2. For this first series of simulations, we use a cell size of Δz = 1 mm across the 2.2 cm A-K gap of each cavity feed. We use a non-uniform radial grid with the highest resolution, Δr = 0.5 mm, at the radial cathode emission surfaces, and Δr = 1 mm at the insulators. We use a slanted dielectric surface model to simulate the 45° insulator surfaces without having any "stairsteps". Each surface cell has a slanted dielectric/vacuum boundary connecting opposite corners of the cell. For these simulations, electrons incident on an insulator are killed at the surface and removed. We use a triangular weighting scheme to avoid leaving behind any charge at the vacuum corner of the cell when a particle is killed [5]. However, the electric

* Sandia National Laboratories is a multi-program laboratory managed and operated by Sandia Corporation, a wholly owned subsidiary of Lockheed Martin Corporation, for the U.S. Department of Energy's National Nuclear Security Administration under contract DE-AC04-94AL85000.
ξ email: tdpoint@sandia.gov

field is consistent with the particle charge remaining on the surface, since $div(\mathbf{E}) = (\rho_{kill} + \rho_{particles})/\varepsilon_0$. If a large number of electrons are killed on the surface, charge buildup would lead to a large electrostatic field repelling other electrons. In this case, accurately simulating the surface would need a model to deal with electron transport and/or breakdown in the dielectric. Fortunately, this is not necessary for these simulations, since we will later show that no electrons hit the insulators. All simulations use the large area diode load shown in Fig. 1.

Figure 2. (a) The full simulation geometry with 21 feed lines and a large area diode load (note extreme aspect ratio), and (b) a closeup of the section $5.35 < z < 6.4$ m, showing cavities 18 – 21 and the start of the downstream MITL, and also showing MITL diagnostic locations.

Each cavity is modeled with the simple circuit shown in Fig. 3. The main capacitor, $C_0 = 100$ nF, is charged to 150 kV for these simulations. When triggered, the switch resistance R_s falls from 10^5 to 0.2 Ω exponentially with a decay time of 2 ns. The switch inductance is $L_s = 25$ nH, and the resistor modeling core losses is a fixed $R_{loss} = 4$ Ω. Simulations using a single feed discharging into a fixed resistive load are in good agreement with a more detailed circuit model of the cavity.

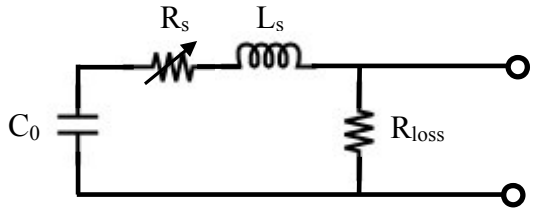

Figure 3. External circuit used to drive the simulation feed lines. The terminals on the right are connected to the two conductors of the 2-D simulation feed.

Electrons are emitted from the cathode using a conventional space-charge-limited emission model. To diagnose power flow and electron loss in the MITL, we define a set of diagnostic locations $\{z_{d,i},\ 1 \le i \le 21\}$ approximately 10 cm downstream of each cavity, shown in Fig. 2b. We save time histories of the voltage, anode and cathode currents, and electron flow current at each location. We also save time histories of electron loss current and power to the anode, feed conductors and insulators divided into "z-bins", where the i'th bin covers $z_{d,i-1} < z < z_{d,i}$. For further detailed analysis of electron loss, we also save all data (**x**,**p**,q,kill-time) of every electron killed in these structures in particle snapshots for later post-processing.

III. RESULTS

Table 2. Parameters for the five simulation setups discussed in the text.

Setup	Emission Threshold (kV/cm)	Feed Timing
1	200	Baseline
2	150	Baseline
3	250	Baseline
4	200	5 ns jitter
5	200	5 ns jitter

Figure 4. Trigger timing delay for each cavity relative to the first.

The results presented here are from the five simulation setups shown in Table 2. Setup 1 is the baseline case: the electron emission threshold is $E_{thr} = 200$ kV/cm, and the feed lines have a trigger timing delay depending on their location relative to the first line, $\Delta t_i = (z_i - z_1)/c$, shown with the red curve in Fig. 4. Setups 2 and 3 simply vary the emission threshold. Finally setups 4 and 5 maintain the 200 kV/cm emission threshold, but add random trigger timing offsets selected from a normal distribution with a 5 ns standard deviation, as shown in Fig. 4. The jitter of the

actual system is 2 ns, much smaller than the random variation used here. Earlier simulations with 2 ns jitter had results almost indistinguishable from the baseline case, so it was decided to increase the jitter to try to affect the behavior more substantially.

The electron distribution from a baseline run at peak power is shown in Fig. 5. Because of field enhancement at stair-stepped corners, two emission cells have turned on across from cavity 6. Electrons emitted from these cells are shown in green. Further emission downstream begins across from cavity 10. Electrons emitted upstream of cavity 13 form turbulent vortices as they pass over the impedance transition. In contrast, electrons emitted downstream of cavity 14 form a relatively smooth sheath.

Figure 5. Electron distribution from a baseline run, color-coded by creation location.

A. Voltage and Current Measurements

Figure 6. Time history of (a) voltage, and (b) anode and cathode current (solid and dashed lines respectively), at MITL locations 6, 13 and 21.

Fig. 6 shows the MITL voltage and currents at three locations from the same baseline run. Peak voltage downstream of cavity 21 is 1.95 MV. The anode and cathode currents show the increase in electron flow moving down the MITL. The load diagnostic locations are shown in Fig. 7. The peak voltage at the load is 1.85 MV. From Fig. 8, we see that an additional ~10 kA of electron flow is launched downstream of MITL location 21. Late in time $I_{c,load} > I_{a,load}$ because electrons emitted from the cathode tip are lost to the outer radial anode surface, upstream of the $I_{a,load}$ location.

Figure 7. Location of voltage and current diagnostics at the load.

Figure 8. Anode and cathode currents at the load and MITL location 21.

There are pronounced differences between the early-time behavior of the five setups. However, by the time of peak power, the differences are greatly reduced. Fig. 9 compares the spatial profile of the electron flow current, time-averaged over a 30 ns window bracketing peak power. The flow current is very similar for the last 9 MITL locations. Setup 2 moves the minimum z-location for emission slightly upstream, while increasing E_{thr} to 250 kV/cm in setup 3 completely suppresses emission from the stair-stepped corners of the first impedance transition. In all cases, we can see a decrease in the flow current at the transitions where the MITL impedance increases.

Figure 9. Spatial profile of the electron flow current at the 21 MITL locations, averaged over 90 < t < 120 ns (i.e. bracketing peak power) for the five setups. The dashed lines are at the center of MITL sections 2 and 3.

B. Electron Loss to the Anode and Insulators

Figure 10. Total electron (a) charge, and (b) energy deposited into the 21 *z-bins* on the anode and insulators along the MITL for the five setups. The off-scale values for *z-bin* 6 of setup 2 are 387 μC and 144 J.

Fig. 10 provides a concise summary of where the electrons are being lost to the anode and insulators along the MITL. The largest losses occur in *z-bins* 6 and 13, which overlap the upstream end of the two impedance transitions. The loss into bin 6 for setup 2 is by far the largest. However, the peak temperature increase on the anode is only 9 ^{o}C, assuming pure aluminum. The value for the Al 6061 actually used differs slightly, but it is clear that electron deposition heating of the anode is completely negligible. Fig. 11 compares the time history of the current loss to bin 6 for the five setups. Of course, the loss is zero for setup 3. The peak current for setup 2 is only a factor of two larger than the others. With $E_{thr} \geq 200$ kV/cm the line insulates everywhere within 20 – 30 ns, and stays insulated until late in the pulse, t > 200 ns. However, for setup 2, there is a sustained loss to the anode throughout the power pulse.

Figure 11. Time history of the current loss into *z-bin* 6 for the five setups.

Figure 12. Plots with time history of the MITL voltage, and V_{crit} as computed by Eq. (1) from the MITL anode current at (a) location 6 for setup 2, and (b) location 13 for setup 3. Also shown is the electron loss current in the *z-bin* immediately upstream of this location.

The key difference between setup 2 and the others is that electrons are emitted from the last few cm of the Z = 16.3 Ω section of the MITL, and electrons are less strongly insulated here than anywhere else. Single particle analysis, based on conservation of energy and azimuthal canonical momentum, shows that electrons are prevented from reaching the anode when $V < V_{crit}$, where

$$\frac{eV_{crit}}{mc^2} = \left[1 + \left(\frac{eA}{mc}\right)^2\right]^{1/2} - 1, \quad (1)$$

where A is the difference between the anode and cathode vector potential. For a uniform coaxial line,

$$A = \int_{r_i}^{r_o} B_\phi(r)dr = IZ_{vac}/c. \quad (2)$$

Fig. 12 shows the time history of V_{mitl} and V_{crit} computed from Eqs. (1) and (2) for two cases: location 6 for setup 2 and location 13 for setup 3. The electron emission upstream of these two cases is topologically identical: only from the uniform MITL section immediately upstream and the first few cm of the impedance transition. We see that the setup 2 case is marginally insulated, and the disruption caused by the abrupt impedance transition is sufficient to sustain a small loss current. In contrast, V_{mitl}/V_{crit} is relatively smaller for setup 3 and the MITL is fully insulated very quickly.

Figure 13. Distribution of electrons lost to the anode near cavity 19 from a baseline run. The dashed lines are the boundaries of *z-bin* 19.

A very encouraging result of these simulations is that there is no electron loss to the insulators. In fact, not even a single electron particle hits the insulators in any simulation. Two independent diagnostics confirm this: the first is a time history diagnostic collecting electrons killed on the insulator surface, and the second saves all particles killed on the anode and the insulators. Results from the second diagnostic are shown in Fig. 13 for cavity 19 from a baseline run. This cavity has electrons killed closer to the insulator than any other, but only on the cavity feed anode, and more than 2 cm from the insulator.